Space–time cloaks through birefringent Goos–Hänchen shifts

Humayun Khan[1], Muhammad Haneef[1,*], and Bakhtawar[1,2]

[1]*Laboratory of Theoretical Physics, Department of Physics, Hazara University Mansehra, 21300, Pakistan*
[2]*Department of Physics, Women University Mardan, 23200, Pakistan*
**Corresponding author: haneef.theoretician@gmail.com*

Received October 28, 2018; accepted November 29, 2018; posted online February 28, 2019

We report a theoretical demonstration for the creation of space–time holes based on birefringence of reflection, transmission, and the Goos–Hächen (GH) shifts from a chiral medium. We observed space–time holes in the reflection, transmission, and their corresponding GH-shifted beams. Two space–time holes are clearly detected in the regions of $0 < t \le 5\tau_0$ and $-5w \le y \le 5w$, as well as in the regions of $-5\tau_0 \le t \le 0$ and $-5w \le y \le 5w$. These space–time holes hide objects and information contents from observers and hackers. The objects and information contents are completely undetectable, and thus events can be cloaked. The results of this paper have potential applications in the invisibility of drone technology and secure communication of information in telecom industries.

OCIS codes: 270.0270, 270.1670.
doi: 10.3788/COL201917.032701.

Light matter interaction at the nanoscale has received enormous attention from scientists[1–9]. Birefringent materials split light beams into two polarization components that propagate at different speeds. Birefringence is measured as the difference of refractive indices of the component beams within the optical material[10]. Birefringence can be induced by external fields when they are applied to optical materials. There are various interesting applications of birefringence, for example, in TV screens, computer monitors, flat panels of mobile phones, automotive devices, and projectors[11].

Birefringence has also been used to create temporal cloaking[4,12–14]. The process of manipulating the speed of light in such a way that a time gap is created in it is called temporal or event cloaking. An event occurring in the time gap is cloaked (hidden) from the detectors. The time gap is then closed so that a specific observer could receive the information of light in its original form. The ability to hide events opens a number of new exciting possibilities in quantum optics[15]. Temporal cloaking has largely been studied theoretically[16,17] as well as experimentally[18]. The temporal cloaking device has significant applications in communication schemes; it also provides better shielded information from noise corruption[19].

The Goos–Hänchen (GH) shift refers to the lateral shift of a light beam from its usual geometric path at the interface of two different media[20,21]. The GH shift has been studied extensively[9,22–25], which has resolved the discrepancy between wave and geometric optics. Numerous configurations have been proposed to enhance the GH shift, such as the asymmetric double-prism configuration[26], layered structure with weakly absorbing medium[27], prism-waveguide coupling system[28], and tunable bidirectional terahertz switch[3]. Yin *et al.*[29] described a surface plasmon resonance configuration, with which a GH shift of about 50 wavelengths was observed. The GH shift in an optical beam has many interesting technological applications. In optical heterodyne sensors, GH shifts can be used to measure various quantities, such as displacement, beam angle, refractive index, film thickness, and temperature[30]. The GH shift shows significant applications in various fields, such as acoustics, micro-optics, nano-optics, and plasma physics[31–33].

An ideal invisibility cloak makes objects disappear if viewed in three-dimensional space. The disappearance is possible for any polarization of the light wave in reflection, as well as in transmission and for a broad range of carrier frequencies of light. There have been mainly two kinds of invisibility cloaks proposed: carpet cloaks and free-space cloaks. A free-space cloak is a designed material shell covering an object in free-space, which can guide the waves to propagate around the shell and make the object invisible. This can lead to hiding drones and automobiles on the ground, etc.[34,35].

A large number of research articles are published on space cloaking, temporal cloaking[36,37], and space–time cloaking, in which different techniques are used to modify invisibility cloaks, temporal time gaps, and event space–time gaps. There is no work on space–time cloaks in which birefringent beams of transmission, reflection, and GH shifts have been used to modify and control the space–time holes for event cloaking. In this article, we use the birefringent beams of transmission, reflection, and GH shifts to create the space–time holes in which the event is cloaked for invisibility as well as information hacking. For this purpose, we consider the chiral atomic medium and calculate the birefringent beams of reflection and transmission, as well as GH shifts.

The space–time hole is created in the birefringent beams of reflection and transmission intensities, and significant space–time holes for event cloaking are found. Our results provide a direction for future experiments for concealing objects and information from viewers and hackers, respectively.

The four-level atomic system, as shown in Fig. 1, is considered. The electric probe field E_p is coupled between states $|2\rangle$ and $|4\rangle$. States $|1\rangle$ and $|3\rangle$ are coupled with magnetic field B_m. States $|3\rangle$ and $|4\rangle$ are coupled with a resonance electric control field E_c. The Rabi frequencies of these fields are $\Omega_{p,m,c}$.

The self Hamiltonian of the system is

$$H_0 = \sum_{i=1}^{4} \hbar\omega_i |i\rangle\langle i|. \tag{1}$$

The Hamiltonian in the interaction picture for this system is written as

$$H_I = \sum_{i=1}^{4} \hbar|i\rangle\langle i| - \frac{\hbar}{2}[\Omega_c e^{-i\omega_c t}|4\rangle\langle 3| + \Omega_p e^{-i\omega_p t}|4\rangle\langle 2| + \Omega_m e^{-i\omega_m t}|3\rangle\langle 1| + \text{h.c.}], \tag{2}$$

where $\Omega_p = \varrho_{42} e^{i\varphi_1} E_0/\hbar$, $\Omega_m = \mu_{31} e^{i\varphi_2} B_0/\hbar$, μ_{31} is the magnetic dipole moment between states $|3\rangle$ and $|1\rangle$, and ϱ_{42} is the electric dipole moment between states $|4\rangle$ and $|2\rangle$. These dipole moments are related to atomic decays as $\mu_{31} = \sqrt{3c^2\hbar\lambda^3\gamma_b/8\pi^2}$ and $\varrho_{42} = \sqrt{3\hbar\lambda^3\gamma_e/8\pi^2}$.

The general form of the density matrix equation is written as

$$\dot{\rho} = -\frac{i}{\hbar}[H_i, \rho] - \sum \frac{1}{2}\gamma_{mn}(a^\dagger a\rho + \rho a^\dagger a - 2a\rho a^\dagger), \tag{3}$$

where $a^\dagger$ represents the rising operators, while a represents the lowering operators. γ_{mn} represents the decays between the states. Using the master equation, we obtain the following coupling rates equations:

$$\dot{\tilde{\rho}}_{31} = \left(\Delta_p - \frac{1}{2}\gamma_b\right)\tilde{\rho}_{31} - \frac{i}{2}\Omega_c^*\tilde{\rho}_{41} - \frac{i}{2}\Omega_m(\tilde{\rho}_{11} - \tilde{\rho}_{33}), \tag{4}$$

$$\dot{\tilde{\rho}}_{41} = \left[i\Delta_p - \left(\frac{1}{2}\gamma_1 + \gamma_e\right)\right]\tilde{\rho}_{41} - \frac{i}{2}\Omega_c\tilde{\rho}_{31} - \frac{i}{2}\Omega_p\tilde{\rho}_{21} + \frac{i}{2}\Omega_m\tilde{\rho}_{43}, \tag{5}$$

$$\dot{\tilde{\rho}}_{42} = \left[\Delta_p - \frac{i}{2}(\gamma_e + \gamma_1)\right]\tilde{\rho}_{42} - \frac{i}{2}\Omega_c\tilde{\rho}_{32} - \frac{i}{2}\Omega_p(\tilde{\rho}_{22} - \tilde{\rho}_{44}), \tag{6}$$

$$\dot{\tilde{\rho}}_{32} = \left(i\Delta_p - \frac{1}{2}\gamma_b\right)\tilde{\rho}_{32} - \frac{i}{2}\Omega_c^*\tilde{\rho}_{42} - \frac{i}{2}\Omega_m\tilde{\rho}_{12}. \tag{7}$$

For weak probe fields, $\Omega_{p,m} \ll \Omega_c, \gamma_1, \gamma_e$. The zero-order coherence terms $\tilde{\rho}_{11}^{(0)}$, $\tilde{\rho}_{22}^{(0)}$, $\tilde{\rho}_{12}^{(0)}$, and $\tilde{\rho}_{21}^{(0)}$ become equal to zero due to small Rabi oscillation. The solutions of Eqs. (4)–(7) are written as

$$\tilde{\rho}_{31}^{(1)} = \frac{\Omega_m}{2W_1}\tilde{\rho}_{11}^{(0)} + \frac{\Omega_p}{4W_1}\frac{\Omega_c^*}{\Delta_p - i(\gamma_1 + \gamma_e)/2}\tilde{\rho}_{21}^{(0)}, \tag{8}$$

$$\tilde{\rho}_{42}^{(1)} = \frac{\Omega_p}{2W_2}\tilde{\rho}_{22}^{(0)} + \frac{\Omega_m}{4W_2}\frac{\Omega_c}{\Delta_p - i\gamma_b/2}\tilde{\rho}_{12}^{(0)}, \tag{9}$$

$$W_1 = \Delta_p - \frac{i\gamma_b}{2} - \frac{|\Omega_c|^2}{4\left(\Delta_p - i\frac{\gamma_1+\gamma_e}{2}\right)}, \tag{10}$$

$$W_2 = \Delta_p - \frac{i(\gamma_e + \gamma_1)}{2} - \frac{|\Omega_c|^2}{4\left(\Delta_p - i\frac{\gamma_b}{2}\right)}. \tag{11}$$

But, in this case, the atoms are prepared in the coherent superposition of states $|1\rangle$ and $|2\rangle$, which are written as

$$|\psi\rangle = \sqrt{x}|2\rangle + \sqrt{1-x}e^{i\varphi}|1\rangle. \tag{12}$$

The zeroth-order density matrix is then $\tilde{\rho} = |\psi\rangle\langle\psi|$. So,

$$\tilde{\rho}_{11,22,12,21}^{(0)} = 1 - x, x, \sqrt{x(1-x)}e^{i\varphi}, \sqrt{x(1-x)}e^{-i\varphi}.$$

The expression for magnetization and polarization in a chiral atomic medium at the probe field's frequency is written as $P = N\varrho_{24}\tilde{\rho}_{42}^{(1)}$ and $M = N\mu_{13}\tilde{\rho}_{31}^{(1)}$, plugging the values of $\tilde{\rho}_{31}^{(1)}$ and $\tilde{\rho}_{42}^{(1)}$ from the Eqs. (8) and (9) in the magnetization and electric polarizations; then, the above equations become $P = \alpha_{EB}B_0 + \alpha_{EE}E_0$ and $M = \alpha_{BB}B_0 + \alpha_{BE}E_0$, where $\alpha_{EE,EB,BE,BB}$ are the following:

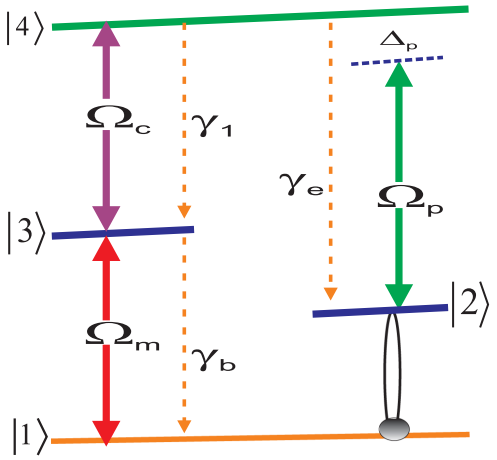

Fig. 1. Energy diagram of four-level atomic system.

$$\alpha_{EE} = \frac{N\varrho_{42}^2 \tilde{\rho}_{22}^{(0)}}{\hbar W_2}, \tag{13}$$

$$\alpha_{BB} = \frac{N\mu_{31}^2 \tilde{\rho}_{11}^{(0)}}{\hbar W_1}, \tag{14}$$

$$\alpha_{BE} = \frac{N\mu_{31}\varrho_{42}|\Omega_c| e^{i(\varphi_2-\varphi_1)}\rho_{21}^{(0)} e^{-i(\varphi+\varphi_c)}}{2\hbar W_1\left[\Delta_p - \frac{i(\gamma_1+\gamma_e)}{2}\right]}, \tag{15}$$

$$\alpha_{EB} = \frac{N\mu_{31}\varrho_{42}|\Omega_c| e^{i(\varphi_1-\varphi_2)}\rho_{21}^{(0)} e^{i(\varphi+\varphi_c)}}{2\hbar W_1\left[\Delta_p - \frac{i(\gamma_1+\gamma_e)}{2}\right]}, \tag{16}$$

where $B = \mu_0(M + H)$, and we obtain electric polarization and magnetization. The electric and magnetic polarizations in the form of chiral coefficients are written by $P_e = \epsilon_0\chi_e^{(1)}E + \frac{\xi_{EH}H}{c}$ and $M = \chi_m^{(1)}H + \frac{\xi_{HE}H}{\mu_0 c}E$. To evaluate the electric and magnetic susceptibilities for the system, we define the electric polarization of the medium as $P_e = \epsilon_0\chi E$, and due to the coherence of the probe field, the polarization is $P_e = |\mathcal{P}_{42}|^2\tilde{\rho}_{24}$, where $\tilde{\rho}_{24}$ and $\mathcal{P}_{42}$ are the dipole matrix elements. Comparing the polarization and magnetization equations, the first-order complex electric and magnetic susceptibilities and chiral coefficients are evaluated for the atomic system as

$$\chi_e = \frac{\alpha_{EE} + \mu_0(\alpha_{EB}\alpha_{BE} - \alpha_{BB}\alpha_{EE})}{\epsilon_0(1 - \mu_0\alpha_{BB})}, \tag{17}$$

$$\chi_m = \frac{\mu_0\beta_{BB}}{1 - \mu_0\beta_{BB}}, \tag{18}$$

$$\xi_{EH} = \frac{c\mu_0\beta_{EB}}{1 - \mu_0\beta_{BB}}, \tag{19}$$

$$\xi_{HE} = \frac{c\mu_0\beta_{BE}}{1 - \mu_0\beta_{BB}}. \tag{20}$$

The light beam incident to a chiral medium becomes birefringent. The divided beams have left and right circular polarization, having refractive indices $n_r^{(-)}$ and $n_r^{(+)}$. The refractive index is calculated for birefringent beams as

$$n_r^{(\pm)} = \sqrt{(1+\chi_e)(1+\chi_m) - \frac{(\xi_{EH}+\xi_{HE})^2}{4}} \pm i\frac{\xi_{EH}-\xi_{HE}}{2}. \tag{21}$$

The group index is written as $\mathrm{Re}\left(n_r^{(\pm)} + \omega\frac{\partial n_r^{(\pm)}}{\partial\Delta_p}\right)$. The group velocity is written as $v_g^{\pm} = c/n_g^{(\pm)}$, while the time of the pulses is written as $t^{(\pm)} = \frac{L}{c}n_g^{(\pm)}$. The propagating probe beam can be reflected back and transmitted through the cavity with a lateral shift. The positive and negative shifts in the probe beam depend upon the dispersive properties of the atomic medium. The GH shifts in the reflection and transmission beams are calculated by the stationary phase theory as $S_{t,r} = -\lambda \mathrm{d}\varphi(T,R)/2\pi\mathrm{d}k_k$ and $k_y = k\sin\theta$, where $\varphi(T,R)$ is the phase associated with transmission or reflection coefficients, and θ is the incident angle. The reflection in the probe beam can be written in a more explicit form as

$$R^{\pm} = \frac{\cos\alpha^{\pm}(Q_0^2 - Q_1^2)Q_1 Q^{\pm}\sin 2\alpha_1 + H_3\sin\alpha^{\pm}}{Q_1 Q_2 H_1\cos\alpha^{\pm} + H_2\sin\alpha^{\pm}}, \tag{22}$$

where α_1, $\alpha^{\pm}$, $Q_{0,1}$, $Q^{\pm}$, and H_{1-4} are written in Appendix A. The sum of reflection and transmission coefficients is equal to one, i.e., $R + T = 1$. The GH shifts in the birefringence reflection and transmission probe beams are written in explicit form as

$$S_{(t,r)}^{\pm} = -\frac{\lambda}{2\pi|T^{\pm}, R^{\pm}|^2}\left[\mathrm{Re}(T^{\pm}, R^{\pm})\frac{\partial}{\partial k_y}\mathrm{Im}(T^{\pm}, R^{\pm}) - \mathrm{Im}(T^{\pm}, R^{\pm})\frac{\partial}{\partial k_y}\mathrm{Re}(T^{\pm}, R^{\pm})\right]. \tag{23}$$

The incident probe beam at the plane $z = 0$ is written as

$$E_i(y,t)|_{z=0} = \frac{1}{2\pi}\int_{-\infty}^{\infty}\int_{-\infty}^{\infty} A(k_y,\Delta_p)e^{i(k_z z + k_y y)}e^{-i\Delta_p t}\mathrm{d}k_y\mathrm{d}\Delta_p, \tag{24}$$

$$A(k_y,\Delta_p) = \frac{W_y}{\sqrt{2\tau_0}}e^{-\frac{W_y^2(k_y-k_{y0})^2}{4}}e^{-\frac{\tau_0^2\Delta_p^2}{4}}. \tag{25}$$

The transmission and reflection beams are written as

$$E_t(y,t) = \frac{1}{2\pi}\int_{-\infty}^{\infty}\int_{-\infty}^{\infty} T(k_y)A(k_y,\Delta_p) \times e^{i[k_z(z-L)+k_y y]}e^{-i\Delta_p(t-t^{(\pm)})}\mathrm{d}k_y\mathrm{d}\Delta_p, \tag{26}$$

$$E_r(y,t) = \frac{1}{2\pi}\int_{-\infty}^{\infty}\int_{-\infty}^{\infty} R(k_y)A(k_y,\Delta_p) \times e^{i(-k_z z + k_y y)}e^{-i\Delta_p(t-t^{(\pm)})}\mathrm{d}k_y\mathrm{d}\Delta_p, \tag{27}$$

where $2d_1 + d_2 = L$ is the length of the cavity.

The birefringence of reflection, transmission, and GH shifts is discussed in this article on the basis of chiral medium. The space–time cloaking on the basis of birefringence reflection and transmission is the main aim of this article. The atomic units are used throughout in this work. The decays rates γ are chosen as 36.1 MHz, and all other parameters are scaled to this γ.

In Fig. 2, the plots are traced for birefringence reflection $R^{\pm}$ and transmission $T^{\pm}$ coefficients versus incident angle θ. The red lines show the birefringence reflection, and the blue lines show the birefringence transmission spectra. The reflection beam is split into the birefringent through a chiral medium shown by red solid and dashed lines. The transmission beam is also split into the birefringent through the chiral medium shown by blue solid and

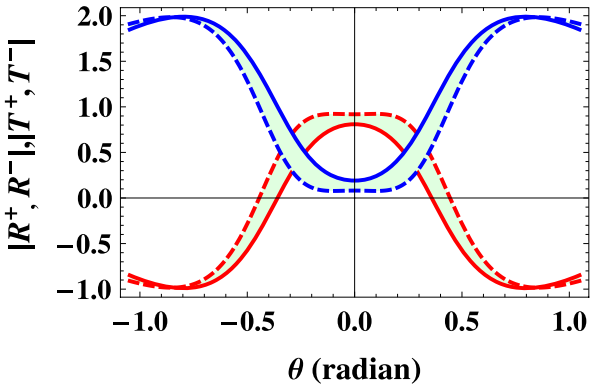

Fig. 2. Birefringent reflection and transmission versus θ, such that $\gamma_{e,1} = 1\gamma$, $\gamma_b = 0.02\gamma$, $\Omega_c = 1.5\gamma$, $\Delta_p = 0\gamma$, $\varphi_1 = \pi/2$, $\varphi(\varphi_{2,c}) = 0$, $x = 0.5$.

dashed lines. The sum of the reflection and transmission at the point of no birefringence is equal to one, $T + R = 1$. In the region of birefringence, the sum of the reflection and transmission coefficients may or may not be equal to one, $T^{\pm} + R^{\pm} \leq 1$.

In Fig. 3, the birefringent reflection $R^{\pm}$ and transmission $T^{\pm}$ coefficients versus control field Rabi frequency $|\Omega_c|/\gamma$ are shown by red and blue solid and dashed lines. There is no birefringence in the reflection and transmission coefficients at $|\Omega_c| = 0\gamma$. The maximum splitting in the reflection and transmission beams occurs at $|\Omega_c| = \gamma$, and then the splitting decreases to become saturated.

Figure 4 shows the birefringence in GH shifts in the reflection $S_r^{(\pm)}$ and transmission $S_t^{(\pm)}$ beams versus incident angle θ. The birefringent reflection and transmission GH shifts have negative and positive shifts in the chiral medium. In an ordinary medium, there are positive and negative shifts, but in the chiral medium, there are four reflection and four transmission GH shifts. There are positive and negative GH shifts in one birefringence beam and two positive and negative shifts in the other birefringence

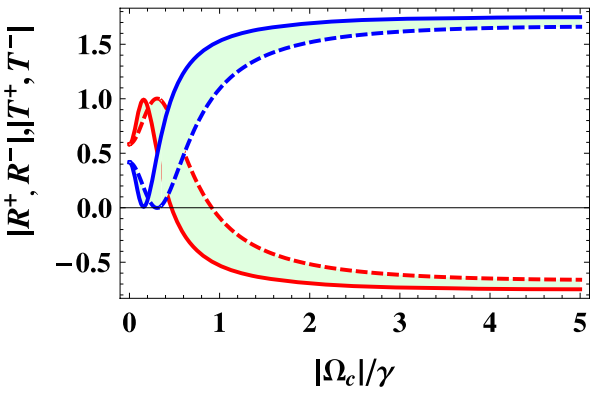

Fig. 3. Birefringent reflection and transmission versus θ, such that $\gamma_{e,1} = 1\gamma$, $\gamma_b = 0.02\gamma$, $\theta = \pi/3$, $\Delta_p = 0\gamma$, $\varphi_1 = \pi/2$, $\varphi(\varphi_{2,c}) = 0$, $x = 0.5$.

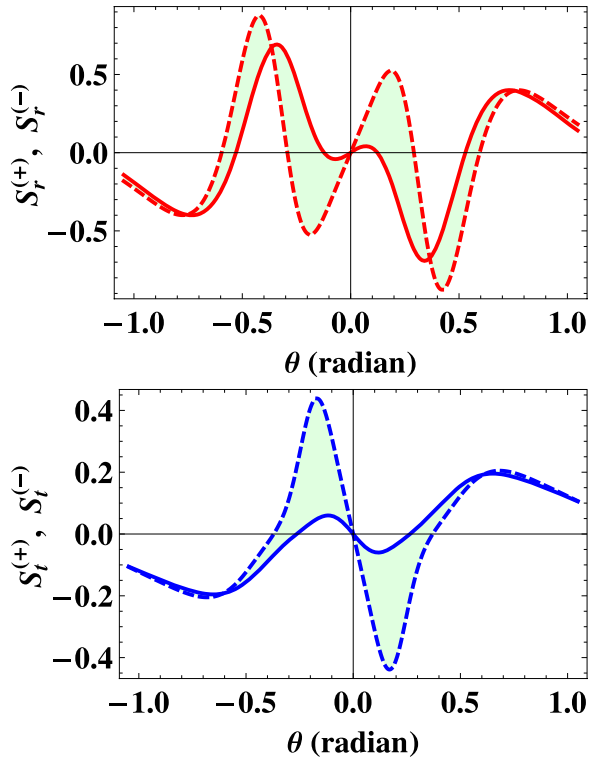

Fig. 4. Birefringence shifts in the reflection beam versus θ, such that $\gamma_{e,1} = 1\gamma$, $\gamma_b = 0.02\gamma$, $\Omega_c = 1.5\gamma$, $\Delta_p = 0\gamma$, $\varphi_1 = \pi/2$, $\varphi(\varphi_{2,c}) = 0$, $x = 0.5$.

beam, as shown in Fig. 4. In the reflection spectrum, the red solid and red dashed lines show the two birefringence beams. Similarly, in the transmission spectrum, the blue solid and blue dashed lines show the two birefringence beams. Each of the birefringence beams in the reflection and transmission spectra has positive and negative parts. The positive part shows a positive GH shift, and the negative part shows a negative GH shift.

Figure 5 shows the birefringence in GH shifts in the reflection $S_r^{(\pm)}$ and transmission $S_t^{(\pm)}$ beams versus control field Rabbi frequency $|\Omega_c|/\gamma$. In this case, the GH shifts in the reflection and transmission beams act as a function of the control fields. The positive and negative GH shifts are calculated with the strength of the control field. At different values of the control field, positive and negative GH shifts are measured for each of the birefringent beams of reflection and transmission.

Figure 6 shows the input pulse intensity normalized to τ_0 and w in the space–time domain, where τ_0 and w are the input pulse widths in time and space, such that $\tau_0 = 1.5$ μs and $w = 30\lambda_p$. The input pulse intensity is taken in a Gaussian form. The Gaussian input pulse incident at a chiral medium splits into birefringence reflection and transmission pulses due to additional contribution of the chiral coefficients.

Figure 7 shows the output pulse intensity of birefringent reflection and transmission pulses normalized with the input pulse widths τ_0 and w in the space–time domain. The birefringent reflection and transmission pulses are

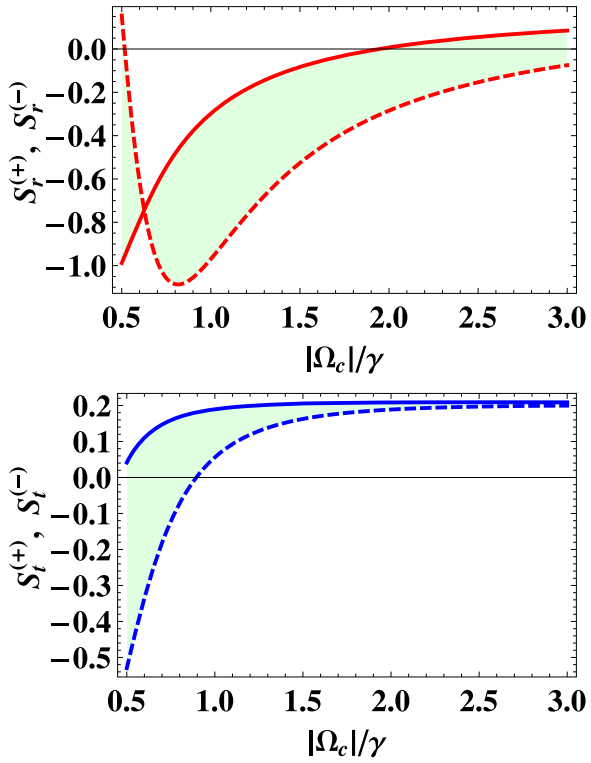

Fig. 5. Birefringence GH shifts in the transmission beam versus θ, such that $\gamma_{e,1} = 1\gamma$, $\gamma_b = 0.02\gamma$, $\theta = \pi/3$, $\Delta_p = 0\gamma$, $\varphi_1 = \pi/2$, $\varphi(\varphi_{2,c}) = 0$, $x = 0.5$.

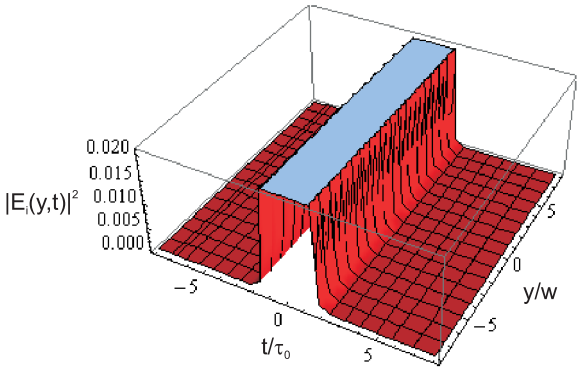

Fig. 6. Normalized input intensity versus t/τ_0 and y/w, $\tau_0 = 1.5$ μs, $w = 30\lambda_p$.

functions of space and time and show intensity variations in space–time domains in such a way that in certain regions of space and time, its intensity vanishes. In these regions of space and time, the pulses are not detected. The space–time holes are created in space and time, where information is not detectable, and an object is not visible. In these space–time holes, the object and information are hidden from outside observers and hackers. This is space–time cloaking.

In conclusion, a four-level chiral atomic medium is used to investigate the birefringent behaviors of reflection, transmission, and GH shifts. The reflection, transmission, and GH shifts split into birefringence beams due to controlling additional contributions of the chiral coefficients.

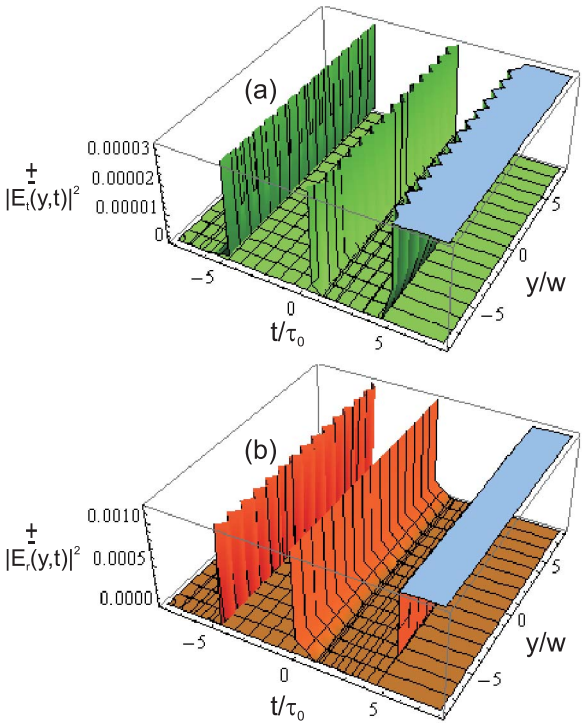

Fig. 7. Normalized transmission and reflection pulses intensities versus t/τ_0 and y/w, such that $\gamma_{e,1} = 1\gamma$, $\gamma_b = 0.02\gamma$, $\theta = \pi/3$, $\Delta_p = 0\gamma$, $\varphi_1 = \pi/2$, $\varphi(\varphi_{2,c}) = 0$, $x = 0.5$, $\Omega_c = 1.5\gamma$, $\tau_0 = 1.5$ μs, $w = 30\lambda_p$.

The birefringent behaviors are controlled and modified with the strength of the control field, probe field detuning, and incident angle. The space–time holes are created in the birefringent beams of reflection/transmission and GH shifts. The information contents and objects are hidden in these space–time holes from outside observers and hackers. In these space holes, information contents and objects are completely undetectable, and the event is cloaked. The results have significant and potential applications in invisible and secure communication of drone technology.

APPENDIX A

$$
\begin{aligned}
Q_{0,1} &= \sqrt{\epsilon_{0,1} - \sin^2\theta},\\
Q^{\pm} &= \sqrt{(n_r^{(\pm)})^2 - \sin^2\theta},\\
\alpha_1 &= d_1 k\sqrt{\epsilon_1 - \sin^2\theta},\\
\alpha^{\pm} &= d_2 k Q^{\pm},\\
H_1 &= 2iQ_0Q_1\cos 2\alpha_1 + (Q_0^2 + Q_1^2)\sin 2\alpha_1,\\
H_2 &= Q_1^2(Q_0^2 + Q_2^2)\cos^2\alpha_1 - (Q_1^4 + Q_0^2Q_2^2)\sin^2\alpha_1\\
&\quad - iQ_0Q_1(Q_1^2 + Q_2^2)\sin 2\alpha_1,\\
H_3 &= Q_1^2(Q_0^2 - Q_2^2)\cos^2\alpha_1 + (Q_1^4 - Q_0^2Q_2^2)\sin^2\alpha_1.
\end{aligned}
$$

References

1. M. Haneef, S. Mohammad, J. Akbar, S. Arif, M. Zahir, and H. Khan, Chin. Phys. Lett. **29**, 073201 (2012).

2. A. Farmani, M. Yavarian, A. Alighanbari, M. Miri, and M. H. Sheikhi, Appl. Opt. **56**, 8931 (2017).
3. A. Farmani, A. Mir, and Z. Sharifpour, Appl. Surface Sci. **453**, 358 (2018).
4. H. Khan, M. Haneef, and Bakhtawar, Chin. Phys. B **27**, 014201 (2018).
5. M. Pu, N. Yao, C. Hu, X. Xin, Z. Zhao, C. Wang, and X. Luo, Opt. Express **18**, 21030 (2010).
6. A. Rahman, I. Ahmad, A. Afaq, M. Haneef, and H. J. Zhao, Chin. Phys. Lett. **28**, 083301 (2011).
7. Bakhtawar, M. Haneef, B. A. Bacha, H. Khan, and M. Atif, Chin. Phys. B **27**, 114215 (2018).
8. M. Haneef, S. Arif, J. Akbar, M. Zahir, and N. Shah, J. Theor. Comput. Chem. **12**, 1350010 (2013).
9. H. Khan and M. Haneef, Can. J. Phys. **96**, 98 (2018).
10. J. A. Danner, T. Tomas, and U. Leonhardt, Nat. Photon. **5**, 357 (2011).
11. P. A. Breddels, in *Proceedings of the 12th International Topical Meeting on Optics of Liquid Crystals* (2007), p. 17.
12. H. Khan and M. Haneef, Laser Phys. **27**, 055201 (2017).
13. M. S. A. Jabar, B. A. Bacha, and I. Ahmad, Laser Phys. **25**, 065405 (2015).
14. M. S. A. Jabar, B. A. Bacha, and I. Ahmad, Chin. Phys. B **25**, 084205 (2016).
15. M. McCall, Contemp. Phys. **54**, 273 (2013).
16. I. Chremmos, Opt. Lett. **39**, 4611 (2014).
17. M. Zhou, H. Liu, Q. Sun, N. Huang, and Z. Wang, Opt. Express **23**, 6543 (2015).
18. R. W. Boyd and Z. Shi, Nature **481**, 35 (2012).
19. Z. Merali, Nat. News, https://doi.org/10.1038/nature.2013.13141.
20. F. Goos and H. Hänchen, Ann. Phys. (Leipzig) **436**, 333 (1947).
21. F. Goos and H. Hänchen, Ann. Phys. (Leipzig) **440**, 251 (1949).
22. S. H. Asadpour, Appl. Opt. **56**, 2201 (2017).
23. S. H. Asadpour, H. R. Hamedi, and M. Jafari, Appl. Opt. **57**, 4013 (2018).
24. G. Solookinejad, M. Panahi, E. A. Sangachin, and S. H. Asadpour, Plasmonics **12**, 849 (2017).
25. S. H. Asadpour, R. Nasehi, H. R. Soleimani, and M. Mahmoudi, Superlati. Microstruct. **85**, 112 (2015).
26. C. F. Li and Q. Wang, Phys. Rev. E **69**, 055601 (2004).
27. H. M. Lai and S. W. Chan, Opt. Lett. **27**, 680 (2002).
28. X. Liu, Z. Cao, P. Zhu, Q. Shen, and X. Liu, Phys. Rev. E **73**, 056617 (2006).
29. X. Yin, L. Hesselink, Z. Liu, N. Fang, and X. Zhang, Appl. Phys. Lett. **85**, 372 (2004).
30. T. Hashimoto and T. Yoshino, Opt. Lett. **14**, 913 (1989).
31. H. K. V. Losch, Optik Stuttgart **37**, 160 (1970).
32. H. K. V. Losch, Optik Stuttgart **32**, 190 (1970).
33. H. K. V. Losch, Optik Stuttgart **32**, 553 (1971).
34. J. B. Pendry, D. Schurig, and D. R. Smith, Science **312**, 1780 (2006).
35. D. Schurig, J. B. Pendry, and D. R. Smith, Opt. Express **14**, 9794 (2006).
36. K. Wu and G. P. Wang, Opt. Express **21**, 238 (2013).
37. P. Y. Bony, M. Guasoni, P. Morin, D. Sugny, A. Picozzi, H. R. Jauslin, S. Pitois, and J. Fatome, Nat. Commun. **5**, 4678 (2014).